Olefin-surface interactions modulate the activity of silica-supported Mo-based olefin metathesis catalysts

*Zachariah J. Berkson,[a] Moritz Bernhardt,[a] Simon Schlapansky,[a] Mathis J. Benedikter,[b] Michael R. Buchmeiser,[b] Gregory Price,[c] Glenn J. Sunley,[c] Christophe Copéret[a]**

[a] Department of Chemistry and Applied Bioscience, ETH Zürich, Vladimir-Prelog-Weg 2, 8093 Zürich, Switzerland

[b] Institute of Polymer Chemistry, Universität Stuttgart, Pfaffenwaldring 55, 70569 Stuttgart, Germany

[c] Applied Sciences, bp Innovation & Engineering, BP plc, Saltend, Hull, HU12 8DS, UK

[*] Corresponding author. Email: ccoperet@ethz.ch

Abstract

Molecularly defined and classical heterogenous Mo-based metathesis catalysts are shown to display distinct and unexpected reactivity patterns for the metathesis of long-chain α-olefins at low temperatures (< 100 °C). Namely, catalysts based on supported Mo oxo species, whether prepared via wet impregnation or surface organometallic chemistry (SOMC), exhibit strong activity dependencies on the α-olefin chain length, with slower reaction rates for longer substrate chain lengths. In contrast, molecular and supported Mo alkylidenes are highly active and do not display such dramatic dependence on chain length. 2D solid-state NMR analyses of post-metathesis

catalysts, complemented by molecular dynamics calculations, evidence that the activity decrease observed for supported Mo oxo catalysts relates to the strong adsorption of internal olefin metathesis products due to interactions with surface Si-OH groups. Overall, this study shows that in addition to the nature and the number of active sites, the metathesis rates and overall catalytic performance depend on product desorption, even in the liquid phase with non-polar substrates. This study further highlights the need to consider adsorption when designing catalysts and the unique activity of molecularly defined supported metathesis catalysts prepared via SOMC.

Introduction

Olefin metathesis is a key technology for the formation of C=C bonds by rearrangement of alkylidene fragments among olefins.[1] Decades of research have yielded highly active and selective olefin metathesis catalysts, largely based on molecular transition-metal (Mo, W, Re and Ru) alkylidenes that are in many instances tolerant to functional groups and widely used in organic and polymer syntheses (Figure 1a).[2–6] By comparison, heterogeneous olefin metathesis catalysts, typically based on supported Mo or W oxides, are industrially used for the upgrading of light olefins[7] but require high-temperature activation and/or harsher reaction conditions.[8] They are composed of ill-defined surface structures with low (<5%) quantities of active sites. These shortcomings have resulted in slow development of heterogeneous metathesis catalysts and limited their broader adoption. Although the nature of the active sites has remained elusive, it is now accepted that isolated, high valent metal oxo species are precursors to the active sites generated *in situ* in the presence of an olefin (Figure 1b).[8] In analogy to the development of homogeneous metathesis catalysts, developing detailed structure-activity relationships for heterogeneous systems has been a

longstanding research objective in order to improve their catalytic performance, scope, and utility.

Towards that goal, surface organometallic chemistry (SOMC) has emerged as a powerful synthetic approach that has been broadly applied for generating well-defined supported olefin metathesis catalysts and pre-catalysts with tailored local environments.[9,10] SOMC involves the grafting of tailored molecular precursors onto solid supports (typically oxides such as silica or alumina), where isolated -OH groups act as anchoring sites for organometallic (or metal-organic) fragments, and enables control of the coordination environment and oxidation state of surface metal sites.[9] By judicious selection of the molecular precursor, the support composition, and the post-grafting treatment, SOMC provides access to well-defined and isolated surface-supported transition metal alkylidene olefin metathesis catalysts,[11–14] as well as monodispersed isolated W and Mo oxo sites as models for oxide catalysts prepared through traditional synthetic approaches.[15,16] For example, highly active and stable olefin metathesis catalysts have been generated by grafting molecular alkylidenes on to dehydroxylated silica (Fig. 1c), preserving the coordination environment of the catalytic center and allowing for a systematic evaluation of the influence of the ligands and nature of the metal on metathesis activity.[11–14] Supported metal alkylidene catalysts prepared by SOMC typically display improved reactivity and stability compared to their molecular analogues,[17] which has been attributed to the isolation of active sites, mitigating bimolecular decomposition pathways that account for the poor stability of many homogeneous catalysts.[18]

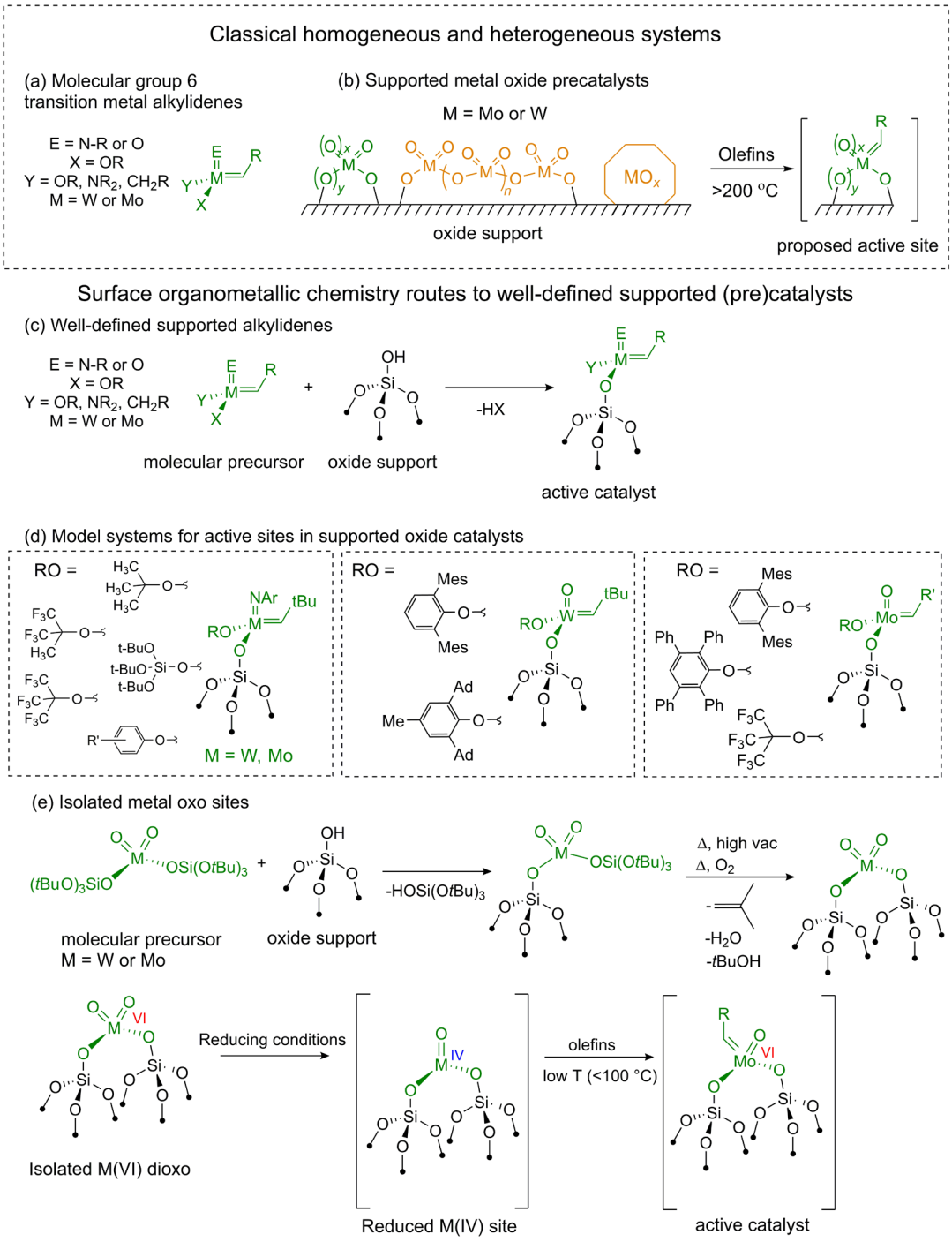

Figure 1. State-of-the-art in olefin metathesis: (a) Molecular group 6 metal alkylidene olefin metathesis catalysts. (b) Surface species proposed on supported Mo or W oxide precatalysts (isolated oxo species, metal oxide polymers, and metal oxide particles) and proposed structure of the active site for olefin metathesis. (c) Surface organometallic chemistry (SOMC) route for grafting of well-defined transition metal alkylidenes onto silica and (d) examples of well-defined supported W and Mo alkylidenes that have been proposed as models for active sites in classical heterogeneous metathesis catalysts. (c) SOMC route for preparation of monodispersed metal oxo sites by grafting of metal oxo siloxides onto silica followed by thermal treatment. These isolated metal oxo sites may be activated for olefin metathesis under reducing conditions, yielding isolated M(IV) centers that react with olefins to form catalytically active species.[15,16]

Recent advances in molecular chemistry have provided access to molecular alkylidenes with ligand sets more similar to the proposed active sites in industrial-type catalysts, which have been stabilized on surfaces by SOMC in order to assess systematically their activity (Figure 1d). These include a series of Mo and W imido alkylidenes[11,14,19] as well as Mo[20,21] and W[22,23] oxo alkylidenes with alkoxide or aryloxide ligands. The resulting supported metal alkylidene catalysts are typically much more active (by several orders of magnitude) for olefin metathesis than supported metal oxide catalysts. Such activity difference have been so far attributed to the specific structure of these well-defined catalysts with their optimized ancillary ligand sets and the high number of active sites (up to 100% in comparison to < 5% for catalysts based on metal oxides). SOMC-based approaches have also been developed to synthesize monodispersed metal (Mo or W) oxo sites on silica as models for industrial-type supported metal oxide catalysts prepared by conventional wet impregnation syntheses. Specifically, grafting of molecular Mo or W oxo siloxides on silica followed by a thermal treatment to remove the organic ligands yields high-valent Mo or W oxo sites. These can be activated under reducing conditions through the generation of M(IV) surface sites that convert *in situ* into catalytically active species in the presence of olefins at low temperatures (< 100 °C), putatively forming M(VI) oxo alkylidenes (Figure 1e).[15,16] These well-defined metal oxo catalysts still exhibit significantly lower activity compared to systems based on well-defined supported alkylidenes. While the number of active sites is certainly a parameter, the large differences in activity suggests that other factors could be at play, for instance dynamics of active species and reaction intermediates. These latter parameters have been largely overlooked until now, though invoked in a few cases to explain the lower catalytic performance of

well-defined supported catalysts in specific reactions. For instance, well-defined supported alkylidenes show poor performance in ring-closing metathesis reactions[24] and supported cationic W oxo alkylidenes display slow initiation for metathesis of internal olefins at very low catalyst loadings.[25] In both cases, restricted dynamics of surface species have been proposed to explain these reactivity patterns.

To that end, we have decided to systematically compare the metathesis activities of a series of supported and molecular Mo-based olefin metathesis catalysts towards long-chain linear a-olefins (C_8-C_{20}) because of their importance to the Shell higher-olefin process (SHOP) and related processes.[26–29] Differences in reactivity patterns among molecular and supported catalysts, including silica-supported and molecular Mo alkylidenes and reduced silica-supported Mo oxos, reveal the importance of olefin-surface interactions on reactivity. Specifically, the supported Mo oxo systems exhibit strong dependencies of activity on chain length, in contrast to the molecularly defined Mo alkylidenes, whether supported or not. Solid-state 2D heteronuclear ^{13}C-^{1}H and ^{29}Si-^{1}H NMR correlation analyses of post-reaction catalysts, with sensitivity enhanced by state-of-the-art fast magic angle spinning (MAS) and ^{1}H detection[30,31] or dynamic nuclear polarization (DNP)[32–34] techniques, complemented by molecular dynamics calculations, uncover the strong adsorption of long-chain olefin metathesis hydrocarbon products onto the silica support near surface -OH sites. These interactions result in decreased reaction rates with increasing chain length in the case of supported Mo oxides due to the stronger adsorption of olefins with increasing chain length.

Results and Discussion

Activity trends of Mo oxo based (pre)catalysts for metathesis of linear α-olefins

We first evaluated the trends in catalyst activity towards metathesis of linear a-olefins for silica-supported Mo oxide-based catalysts. We focused on a broad range of linear a-olefins (C_8-C_{20}) that can be obtained by olefin oligomerization[26,35,36] or Fischer-Tropsch[28,29,37] processes. Primarily molybdenum-based catalysts were tested as they are known to be more efficient for terminal olefin metathesis than their W analogues[11,13] (*vide infra*) due to better tolerance for ethylene.[38] Monodispersed Mo dioxo species (1.56 wt% Mo) were generated via an SOMC approach as previously reported[16] and activated at room temperature by prereduction with 2 equivalents on a per Mo basis of the molecular organosilicon reductant 1-methyl-3,6-bis(trimethylsilyl)-1,4-cyclohexadiene (MBTCD),[15,39] which is denoted **$(\equiv SiO)_2Mo(=O)_2$-red** (Fig. 2a). For comparison, a classical silica-supported Mo oxide catalyst was prepared by an incipient wetness impregnation approach followed by calcination under synthetic air.[40] This oxidized precatalyst contains 3.65 wt% Mo, is also activated for low-temperature metathesis by 2 equivalents of the same organosilicon reductant (MBTCD) and is denoted **MoO_x/SiO_2-red** (Fig. 2b). Both **$(\equiv SiO)_2Mo(=O)_2$** and **MoO_x/SiO_2** contain residual isolated surface Si-OH species, as evidenced by their FTIR spectra in Figures S1 and S2. Based on previous X-ray Adsorption Spectroscopic (XAS) analyses,[16,41] both SOMC and incipient wetness impregnation approaches yield predominantly isolated Mo dioxo surface species, though the activity of the resulting precatalysts is modestly different (*vide infra*) suggesting differences in the quantities of active sites generated.

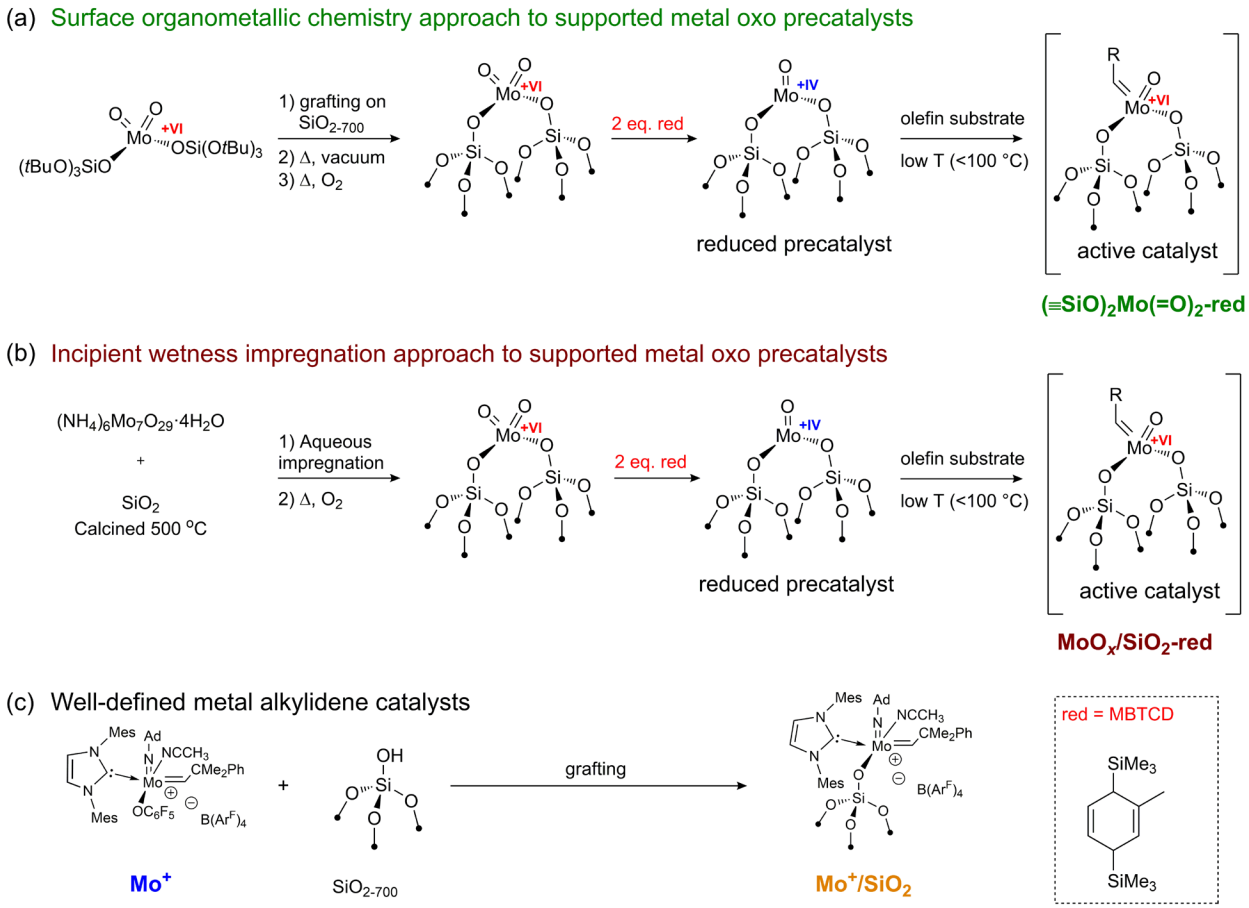

Figure 2. Catalysts and preparation methods: (a) SOMC-based approach to supported metal oxo precatalysts, which are active for low-temperature olefin metathesis using the organosilicon reductant MBTCD, **(≡SiO)$_2$Mo(=O)$_2$-red**. (b) Incipient wetness impregnation approach to metal oxo precatalysts, which are activated for low-temperature metathesis under the same conditions yielding the catalyst **MoO$_x$/SiO$_2$-red**. (c) Well-defined cationic Mo imido alkylidene catalysts in molecular (**Mo$^+$**) and supported (**Mo$^+$/SiO$_2$**) forms.

The reactivities of the catalysts based on metal oxo precatalysts, **(≡SiO)$_2$Mo(=O)$_2$-red** and **MoO$_x$/SiO$_2$-red**, were assessed at both 70 °C and 30 °C. All reactions were conducted in batch mode under N_2 atmosphere. 1,2-Dichlorobenzene was chosen as solvent due its low vapor pressure. Liquid phase olefin metathesis reaction rates for the metal oxo based materials were found to generally depend on the precise reaction conditions, particularly the purity of the olefin stock solutions. Highest reaction rates were observed when the olefin substrates were freshly purified immediately before the catalytic reaction tests according to a rigorous purification protocol[11] (see Experimental Section for details).

Both **(≡SiO)$_2$Mo(=O)$_2$-red** and **MoO$_x$/SiO$_2$-red** are competent for the metathesis of linear α-olefins in the liquid phase at low temperature. For 1-nonene as a prototypical substrate, **(≡SiO)$_2$Mo(=O)$_2$-red** exhibits maximum product formation rates (measured after ca. 10 minutes of reaction time with no observed induction period) of 2.6 and 2.0 (mmol product [mmol Mo]$^{-1}$ [min]$^{-1}$) at 70 °C and 30 °C, respectively (Figures S4 and S5, Table S1). The W-based analogue **(≡SiO)$_2$W(=O)$_2$-red**[15] was also tested at 70 °C for comparison but was found to exhibit lower activity for 1-nonene metathesis with a maximum rate of 0.9 (mmol product [mmol W]$^{-1}$ [min]$^{-1}$) (Figure S6, Table S1). The lower activity of the W based catalyst compared to the Mo analogue is consistent with recent studies on well-defined silica-supported alkylidenes,[11,13] which found that Mo-based catalysts are typically much more active for the metathesis of terminal olefins because of the lower stability of off-cycle square-planar (SP) metallacycle intermediates generated in the presence of ethylene.[38] By comparison, **MoO$_x$/SiO$_2$-red** exhibits initial 1-nonene product formation rates of 3.9 and 0.71 (mmol product [mmol Mo]$^{-1}$ [min]$^{-1}$) at 70 °C and 30 °C, respectively (Figures S7 and S8, Table S1). For both **(≡SiO)$_2$Mo(=O)$_2$-red** and **MoO$_x$/SiO$_2$-red**, significant conversion (6-11%) is observed to internal olefin isomers of the desired 1-nonene metathesis product at 70 °C (Table S1), suggesting formation of Mo hydrides that promote isomerization of the long-chain internal olefins.[42] Improved product selectivities were observed at 30 °C (>98%) compared to 70 °C (Table S1). Additionally, substantial solvent evaporation was observed at 70 °C after long reaction times when open reaction vials were used to allow for release of ethylene. Accordingly, reactions were also run at 70 °C in closed reaction vials, yielding higher initial reaction rates but lower overall conversions (Table S2). The product *E* and *Z* selectivities of the two catalysts based on

silica-supported Mo oxo species, **(≡SiO)$_2$Mo(=O)$_2$-red** and **MoO$_x$@SiO$_2$-red,** were very similar at low conversions, ca. 70% and 30%, respectively (*E*/*Z* ratio ~ 2.1 at 70 °C and ~2.3 at 30 °C, Fig. S9 and S10, Table S1). Since stereoselectivity in olefin metathesis at low conversions depends directly on the structure of the active site,[43,44] these similar values corroborate that both catalysts have similar active site structures.

To assess the influence of olefin chain length on activity, **(≡SiO)$_2$Mo(=O)$_2$-red** was tested as a catalyst for the metathesis of the linear α-olefins 1-octene, 1-nonene, 1-tridecene, 1-hexadecene, and 1-eicosene. Maximum product formation rates of 9.9, 7.8, 4.5, 2.7, and 0.9 (mmol product [mmol Mo]$^{-1}$ [min]$^{-1}$) at 70 °C (in closed reaction vials) and 3.2, 2.6, 2.0, 1.6, and 0.4 (mmol product [mmol Mo]$^{-1}$ [min]$^{-1}$) at 30 °C (in open reaction vials) were observed after 10 minutes reaction time. Lower substrate concentrations (0.5 M) were used for the 1-eicosene reaction tests to mitigate the poor solubility of the very long-chain metathesis product. The initial product formation rates are compared in Figure 3a, the kinetic profiles are shown in Figures S11-S20, and results are summarized in Tables S2 and S3. **MoO$_x$@SiO$_2$-red** was also tested for 1-nonene, 1-tridecene, and 1-hexadecene metathesis at 30 °C and showed similar trends to **(≡SiO)$_2$Mo(=O)$_2$-red**, though with somewhat lower activity on a per Mo basis and in some cases a slight induction period (Figures S21-S23, Table S4). As shown in Figure 3a, reaction rates for **(≡SiO)$_2$Mo(=O)$_2$-red** decrease monotonically as a function of olefin chain length for the entire substrate series studied here at both 70 °C and 30 °C. While **(≡SiO)$_2$Mo(=O)$_2$-red** exhibits promising activity and selectivity overall for metathesis of linear α-olefins at low temperature (<100 °C), we sought to understand the origin of its reduced metathesis activity for long-chain

terminal alpha olefins and so compared the reactivity to that of well-defined metal alkylidene-based catalysts.

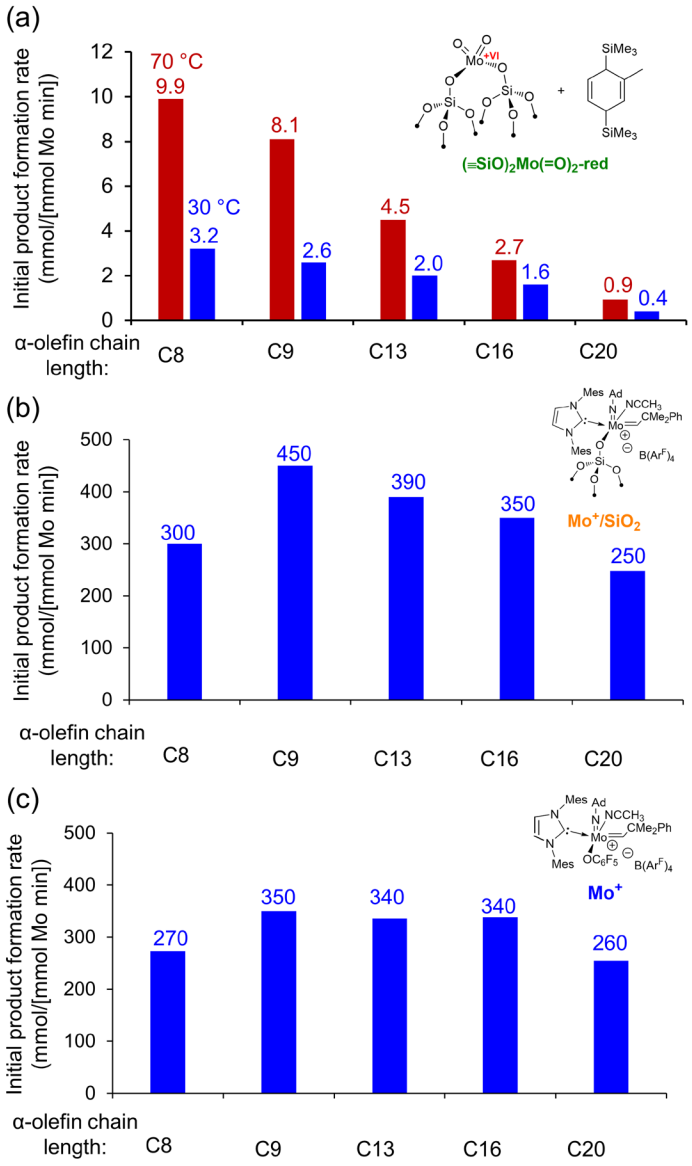

Figure 3. Initial product formation rates for metathesis of linear alpha olefins catalyzed by (a) **(≡SiO)$_2$Mo(=O)$_2$-red** at 70 °C (red) and 30 °C (blue) or well-defined Mo alkylidene catalysts (b) **Mo$^+$/SiO$_{2\text{-}700}$** or (c) molecular **Mo$^+$**. All reactions were carried under an N_2 atmosphere, in closed (70 °C) or open (30 °C) batch reactors containing 2.5 mL of substrate stock solution in 1,2-dichlorobenzene. 1 M substrate stock solutions were used for 1-octene, 1-nonene, 1-tridecene, and 1-hexadecene, with substrate: Mo ratios of ca. 1000:1 for **(≡SiO)$_2$Mo(=O)$_2$-red** and ca. 5000:1 for **Mo$^+$** and **Mo$^+$/SiO$_{2\text{-}700}$**. For 1-eicosene, a 0.5 M substrate stock solution was used with substrate: Mo ratios of ca. 500:1 for **(≡SiO)$_2$Mo(=O)$_2$-red** and ca. 2500:1 for **Mo$^+$** and **Mo$^+$/SiO$_2$**.

Activity of well-defined molecular and supported Mo alkylidene olefin metathesis catalysts

To assess the influence of active site structure and surface composition on linear α-olefin metathesis activity, we tested for comparison a well-defined and highly active cationic Mo alkylidene catalyst in both molecular (**Mo**$^{+}$)[45] and silica-supported (**Mo**$^{+}$**/SiO$_2$**)[12] forms (Figure 2c). By comparison to the catalysts based on supported Mo oxides, those based on well-defined Mo alkylidenes (**Mo**$^{+}$ and **Mo**$^{+}$**/SiO$_2$**) exhibited orders of magnitude higher activity at 30 °C with no induction period. While the increased reaction rates can be due to the specific nature and the number of the active sites, it is noteworthy that the initial product formation rates (measured reaction times of 3-4.5 minutes) of 300, 450, 380, 340, and 250 (mmol product [mmol Mo]$^{-1}$ [min]$^{-1}$) for 1-octene, 1-nonene, 1-tridecene, 1-hexadecene, and 1-eicosene, respectively (Figure 3b), were quite similar for **Mo**$^{+}$**/SiO$_{2\text{-}700}$** as a function of substrate chain length. By comparison, the molecular catalyst **Mo**$^{+}$ exhibited similar maximum product formation rates (measured at a reaction time of 3 minutes) of 270, 350, 340, 340, and 260 (mmol product [mmol Mo]$^{-1}$ [min]$^{-1}$) for 1-octene, 1-nonene, 1-tridecene, 1-hexadecene, and 1-eicosene, respectively (Figure 3c). Additional details of the catalytic tests are provided in Figures S24-S33 and Tables S5 and S6. Based on repeated measurements, the uncertainty of these values was estimated to be ± 30 (mmol product [mmol Mo]$^{-1}$ [min]$^{-1}$) (see Fig. S33 for details). In general, the well-defined cationic alkylidene catalysts were highly efficient in both molecular and supported forms: for each of the linear a-olefin substrates tested, **Mo**$^{+}$ and **Mo**$^{+}$**/SiO$_{2\text{-}700}$** reached >40% conversion within the first three minutes of the reaction period. The supported catalyst **Mo**$^{+}$**/SiO$_2$** exhibited equivalent or higher activity for each substrate compared to **Mo**$^{+}$, consistent with previous comparisons of well-defined supported and molecular alkylidenes.[12,17] In contrast

to **(≡SiO)$_2$Mo(=O)$_2$-red** and **MoO$_x$@SiO$_2$-red**, the molecular catalyst **Mo$^+$** showed no significant dependence of activity on substrate chain length, as expected for a homogeneous catalyst based on the above results. By comparison, **Mo$^+$/SiO$_{2\text{-}700}$** exhibited a modest decrease in activity as a function of substrate chain length from 1-nonene to 1-eicosene, similar to but not quite as pronounced as that observed for **(≡SiO)$_2$Mo(=O)$_2$-red** at 30 °C (Figure S34). Based on the catalytic data discussed above, we hypothesized that the differences in reaction trends of the Mo oxo and well-defined alkylidene based catalysts arise in part from differences in surface dynamics relating to the distinct surface compositions of the catalysts.

Metathesis products adsorbed on post-reaction metathesis catalysts

Specifically, solid-state NMR spectroscopy was used to probe the structure, dynamics, and interactions of the organics adsorbed on **(≡SiO)$_2$Mo(=O)$_2$-red** after reaction. Solid-state 2D heteronuclear correlation NMR spectra establish the types of organic species and their surface interactions by leveraging NMR sensitivity enhancements provided by either fast-MAS and ^{1}H detection[30,31] or by dynamic nuclear polarization (DNP).[32–34] For example, Figure 4 shows the solid-state 2D ^{1}H{^{13}C} dipolar heteronuclear multiple quantum correlation (*D*-HMQC) spectrum of **(≡SiO)$_2$Mo(=O)$_2$-red** after 24 h reaction at 30 °C with 1-hexadecene in 1,2-dichlorobenzene (ca. 80% conversion). Prior to the solid-state NMR analysis, the catalyst was washed with benzene to remove weakly bound surface species and dried under high vacuum ($<10^{-5}$ mbar). Fast MAS (50 kHz) and indirect detection provide high ^{13}C NMR sensitivity and resolution, enabling detection of the 2D spectrum of the surface-bound organic species at natural abundance (1.1%) ^{13}C. The 2D ^{1}H{^{13}C} spectrum shows well-resolved correlated signals that can each be assigned to organic

moieties on the catalyst surface. Specifically, the correlated signal at -1 ppm in the ^{13}C dimension and 0.3 ppm in the ^{1}H dimension is assigned to surface -$OSi(CH_3)_3$ moieties resulting from reaction of the organosilicon reductant. The ^{1}H signals at 1.0, 1.5, and 2.2 ppm are each correlated to ^{13}C signals at 13, 21-30, and 32 ppm, respectively, which are assigned to -CH_3, aliphatic -CH_2-, and allylic -CH_2- moieties, respectively, while the ^{1}H signal at 5.6 ppm is correlated to a ^{13}C at 132 ppm and is assigned to internal olefinic species. The absence of ^{13}C or ^{1}H signals from other olefinic species and the relatively narrow linewidth of the ^{1}H signal at 5.6 ppm indicates that only a single type of internal olefin is present at the catalyst surface, most likely the bulky C30 product of 1-hexadecene metathesis, 15-triacontene. Differences between the *E*- and *Z*-stereoisomers likely cannot be resolved by solid-state NMR as they are expected to be separated by <0.1 ppm in ^{1}H NMR and <0.5 ppm in ^{13}C NMR. This internal olefin is strongly sorbed on to the catalyst surface, as further corroborated by ^{1}H T_2 spin-spin relaxation time analyses (Table S7), which are sensitive to the dynamics of the surface species.[46] The T_2 relaxation times of the adsorbed olefins are found to be quite short (< 2 ms) consistent with strong adsorption and hindered dynamics of the surface-bound organics. The 1D and 2D $^{1}H\{^{13}C\}$ MAS NMR spectra and analyses thus establish that the predominant surface-bound organic component on post-reaction **$(\equiv SiO)_2Mo(=O)_2$-red** is the bulky olefin metathesis product, which is likely slow to desorb, thereby limiting catalyst efficiency.

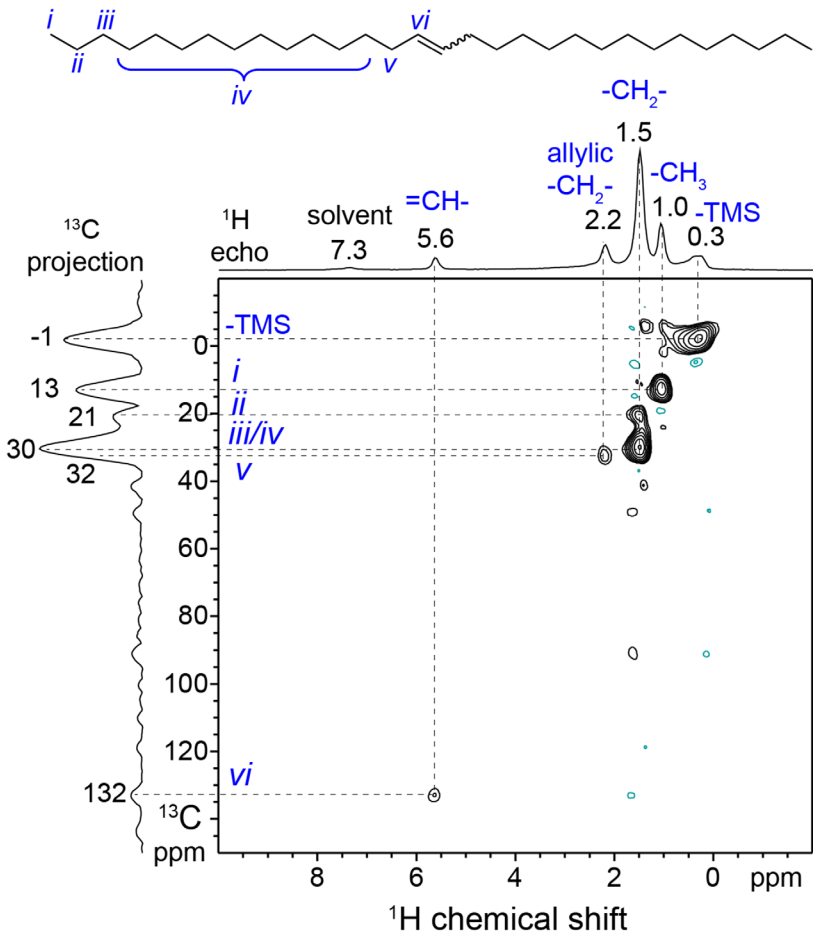

Figure 4. Solid-state 2D $^{1}H\{^{13}C\}$ *D*-HMQC NMR correlation spectrum of **(≡SiO)$_2$Mo(=O)$_2$-red** after 24 h reaction with 1-hexadecene in 1,2-dichlorobenzene at 30 °C, 3x washing with C_6H_6, and drying under high vacuum. The spectrum was acquired at 16.4 T, 50 kHz MAS, 280 K, and with 60 rotor periods (1.2 ms) for ^{13}C-^{1}H recoupling. A 1D ^{1}H echo MAS NMR spectrum acquired under the same conditions is shown along the horizontal axis for comparison. All correlated signals are assigned to surface trimethylsilyl (-TMS) or to the internal olefin product of 1-hexadecene self-metathesis as indicated by the Roman numeral labels on the molecular structure above.

The adsorption of the bulky olefin metathesis products at room temperature appears to be competitive with the 1,2-dichlorobenzene solvent. This is evidenced by comparison of the ^{1}H MAS NMR spectra of **(≡SiO)$_2$Mo(=O)$_2$-red** after 24 h reaction with 1-hexadecene or 1-nonene in Fig. S35. Both spectra exhibit a ^{1}H signal at 7.3 ppm, which is assigned to residual adsorbed 1,2-dichlorobenzene solvent. However, for the catalyst after 1-nonene metathesis this signal was greatly increased in intensity relative to the ^{1}H signals from

adsorbed olefinic species, while for the catalyst after 1-hexadecene metathesis the solvent signal was greatly diminished.

The nature of the olefin-surface interaction was further elucidated by analysis of 2D $^{29}Si\{^{1}H\}$ and $^{13}C\{^{1}H\}$ heteronuclear correlation (HETCOR) spectra by leveraging DNP-NMR techniques at low temperature. DNP-NMR provides greatly enhanced NMR signal sensitivity from surfaces and enables acquisition of 2D NMR correlation spectra that probe organic-inorganic interactions of adsorbed and surface species.[47,48] Though DNP-NMR techniques have been widely used for analysis of diverse organic-inorganic hybrid materials including colloidal nanoparticles[49,50] and catalysts,[51,52] there are surprisingly few examples of its application to characterize molecular adsorption phenomena at surfaces,[53] despite the critical importance of such phenomena for catalysis.

The DNP-enhanced 1D $^{13}C\{^{1}H\}$ CP-MAS spectrum of **(≡SiO)$_2$Mo(=O)$_2$-red** after 4 hours reaction with 1-hexadecene (Fig. S36) shows similar ^{13}C signals to those observed in Figure 3, though slightly broader likely because of slower molecular dynamics under the low-temperature conditions.[46] In addition to the ^{13}C signal at 128 ppm of internal olefinic and/or aromatic species, a ^{13}C signal is detected at 116 ppm from terminal olefinic moieties, evidencing the co-existence of both internal and terminal olefin species adsorbed on the catalyst surface at intermediate reaction times (i.e., low conversions). This suggests that metathesis activity of liquid-phase olefins at low temperatures is largely mediated by adsorption of the olefin substrate and desorption of the internal olefin product, with a pool of adsorbed product molecules building up on the catalyst surface at longer reaction times.

The site-specific interactions of the adsorbed olefin species with the silica support are established by analysis of 2D $^{29}Si\{^{1}H\}$ DNP-HETCOR spectra of post-reaction

(≡SiO)$_2$Mo(=O)$_2$-red acquired with different cross-polarization contact times in Figure 4, which selectively detect ^{1}H-^{29}Si spin pairs that are dipole-dipole coupled through space over sub-nanometer distances. The ^{1}H signals from different moieties of adsorbed organic species are assigned based on the 2D ^{13}C{^{1}H} HETCOR spectrum in Figure S36 and comparison to the room-temperature 2D ^{1}H{^{13}C} *D*-HMQC spectrum in Figure 4 (acquired without DNP). Specifically, the ^{1}H signal at 0.0 ppm is assigned to -TMS moieties based on its correlation in Fig. S36 to a ^{13}C signal at 0 ppm (purple shaded region in Figure S36). The ^{1}H signals at 0.7 to 2.7 ppm are assigned to aliphatic moieties (green shaded regions in Fig. 5 and S36) based on their correlation to ^{13}C signals at 14, 23, and 31 ppm. The ^{1}H signals from 5.8 to 6.4 ppm (grey shaded regions) are assigned to DNP solvent molecules (1,1,2,2-tetrachloroethane) based on their correlation in Fig. S36 to ^{13}C signals at 78 ppm. The ^{1}H signals from 4.4 to 5.6 ppm are correlated in Fig. S36 to the ^{13}C signal at 31 ppm from allylic ^{13}C moieties and are assigned to olefinic moieties. There are no correlations of these signals to the ^{13}C signals from olefinic moieties at 116 and 128 ppm observed in Fig. S36 likely because of their low signal intensity and spectral broadening under the low-temperature measurement conditions. Nevertheless, the signal assignments are corroborated by the correlation of the ^{1}H signal at 5.6 ppm to the ^{13}C signal at 132 ppm in the ^{1}H{^{13}C} *D*-HMQC spectrum acquired at room temperature in Figure 4. Finally, the ^{1}H signals between 7.1 to 8.5 ppm are assigned to aromatic species (e.g., 1,2-dichlorobenzene, blue shaded regions) based on the weak correlation of the ^{1}H signal at 7.1 ppm to the ^{13}C signal at 128 ppm in Figure S36. We note that ^{1}H signals at >7 ppm could also arise in part from strongly hydrogen-bonded or hydrated -OH moieties, as have been previously observed under DNP-NMR conditions for silicate and aluminosilicate zeolites[54,55] and

other silica based materials,[56] though such species are expected to be dilute in the dehydroxylated supported catalyst **(≡SiO)$_2$Mo(=O)$_2$-red**.

Surface Si-OH species act as olefins adsorption sites in **(≡SiO)$_2$Mo(=O)$_2$-red**, as established by analysis of the 2D ^{29}Si{^{1}H} DNP-HETCOR spectra. At short ^{29}Si-^{1}H contact times (0.5 ms, Fig. 5a), weak ^{29}Si signals are detected at -105, -113, and -121 ppm, which are assigned based on literature[54,56] to partially crosslinked Q^3 species and two different types of fully crosslinked surface Q^4 species, respectively. The Q^n notation indicates a silicon atom in a tetrahedral environment bonded to four oxygen atoms, of which n are bonded to another silicon atom and 4-n are incompletely crosslinked, e.g. H terminated. Notably, the ^{29}Si signals at -105 and -113 ppm are correlated with ^{1}H signals at 4.9 and 5.3 ppm from olefinic species, which directly establishes the sub-nanometer proximities and mutual interactions of surface silanols and olefinic moieties of adsorbed molecules, as depicted schematically in the inset to Fig. 5a. The short contact times used make this measurement principally sensitive to interactions over distances of < 0.5 nm, indicating that the olefinic moieties of the surface-bound olefins interact preferentially with surface silanol species over sub-nanometer distances. This is consistent with weak H bonds between the surface silanols and adsorbed olefins, similar to what has been proposed for olefin-methanol H bonds in solution.[57] Indeed, π-H bonds have recently been observed experimentally for olefins adsorbed on hydroxylated silica surfaces.[58,59]

The 2D ^{29}Si{^{1}H} DNP-HETCOR spectra also corroborate the presence of coadsorbed dichlorobenzene molecules and trimethylsiloxy surface moieties. At longer ^{1}H-^{29}Si contact times (5 ms, Fig. 4b), additional correlated signals are detected at 1.8 and 8.1 ppm, which respectively arise from alkyl and aromatic ^{1}H species, consistent with the close proximity

of the aliphatic chains of the long-chain olefins at the silica surface and the co- adsorption of 1,2-dichlorobenzene molecules, respectively. Weak ^{29}Si signals are also detected at 28 and 22 ppm (Figure S37), which are assigned based on their chemical shift positions to two different types of surface -OSi(CH$_3$)$_3$ that are likely byproducts of the reduction process.

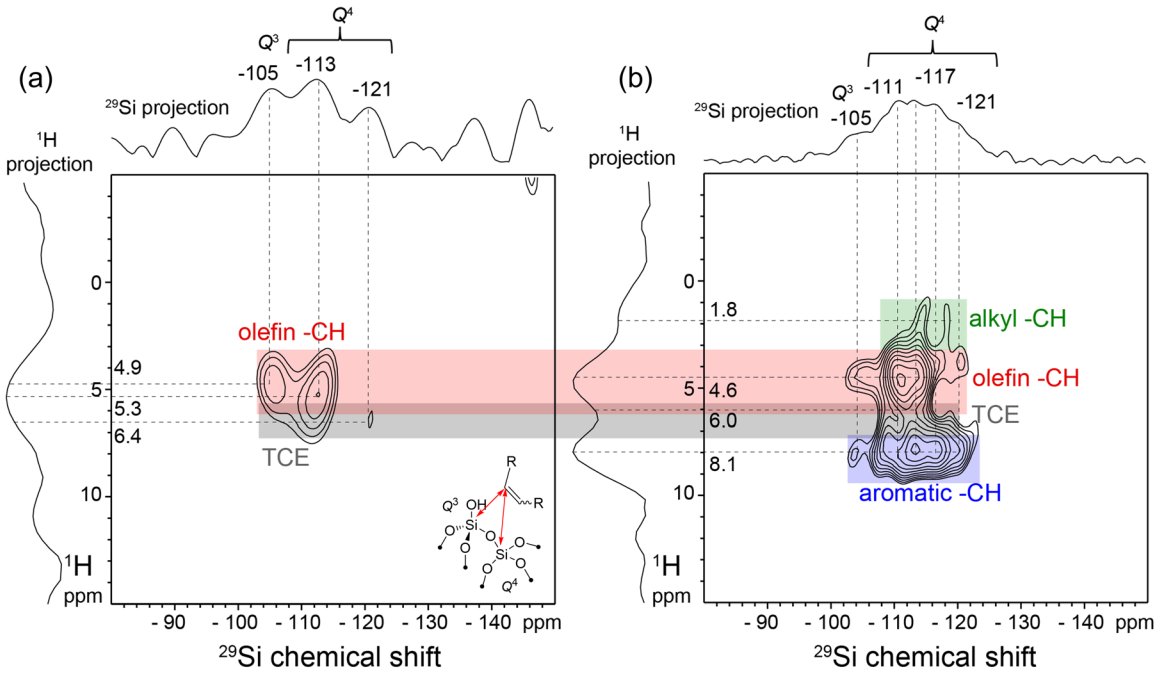

Figure 5. Solid-state 2D ^{29}Si{^{1}H} DNP-HETCOR spectra of **(≡SiO)$_2$Mo(=O)$_2$-red** after 4 h reaction with 1-hexadecene in 1,2-dichlorobenzene at 30 °C, 3x washing with C_6H_6, and drying under high vacuum. The 2D spectra were acquired at 14.1 T, 12.5 kHz MAS, 100 K, under continuous microwave irradiation at 395 GHz, in the presence of 16 mM TEKPol biradical in 1,1,2,2-tetrachloroethane (DNP solvent), and with ^{29}Si-^{1}H contact times of (a) 0.5 ms and (b) 5 ms. The schematic in (a) shows interactions of an olefin moiety with surface Si-OH (Q_3) and fully crosslinked (Q_4) surface silicate species, consistent with the correlated signals in the 2D spectra.

Dynamics and adsorption of olefins on silica

Overall, the solid-state NMR results and analyses evidence that long-chain internal olefin metathesis products adsorb competitively with solvent molecules at surface Si-OH sites. Though substrate-surface interactions have not previously been the subject of detailed analysis in the field of olefin metathesis, it has been recognized that adsorption of olefins importantly influences activity and selectivity. For instance, strong adsorption of olefins on

alumina favors secondary metathesis isomerization reactions in the CH_3ReO_3/Al_2O_3 system, leading to thermodynamic product selectivities for propene metathesis across a broad range of contact times.[43,44] Modification of the alumina surface to passivate surface Al-OH moieties yields non-equilibrium E/Z selectivities.[44] While silica is typically considered a more inert catalyst support than alumina due to the absence of strong Brønsted or Lewis acid sites, there is growing recognition of the importance of surface interactions in modulating reactivity, particularly for challenging substrates. For instance, interactions of functionalized olefins containing ester groups and surface silanol groups were recently found to enrich the near-surface concentration of olefins and influence product selectivities for ring-closing metathesis reactions catalyzed by well-defined cationic Mo alkylidenes supported on mesoporous silicas.[60] The silica-supported Mo oxo system is known to possess strong Brønsted acid sites that could act as adsorption sites,[61] and even on pure silica the interaction energies of hydrocarbons are known to increase as a function of chain length and are greater for alkenes than alkanes.[62] The catalytic reaction tests and solid-state NMR analyses discussed above show that substrate-silica interactions are non-negligible even for long-chain olefinic hydrocarbons and indeed have significant effects on catalytic reaction properties at low reaction temperatures (<100 °C). We sought to understand these effects from a computational perspective as well.

To further understand the influence of surface interactions on olefin adsorption, we conducted molecular dynamics (MD) calculations of internal and terminal linear olefins of varied chain lengths on a periodic surface model of dehydroxylated amorphous silica having approximately 1.1 OH/nm^2.[63] In each case, the olefins appear to be stabilized on the surface by interactions with surface silanols, with the distances between surface -OH and

olefinic carbon atoms ranging from 0.22 to 0.51 nm (Table S8), consistent with the solid-state NMR results discussed above. These distances are within the range expected for olefin-OH hydrogen bonding interactions.[57] Short distances (0.24 to 0.36 nm) are also observed between allylic and aliphatic H atoms and surface siloxane bridges, suggesting that dispersion interactions with surface siloxanes provide additional stabilization of the adsorbed olefins at the surfaces, increasing in strength as a function of chain length. Indeed, the magnitude of the calculated energies of adsorption generally increases as a function of chain length for both terminal and internal olefins (Table S8), with internal olefins exhibiting slightly stronger adsorption energies compared to terminal olefins of the same molecular weight. These trends are qualitatively consistent with measurements of olefin adsorption energies and enthalpies on silica by gas chromatography.[62] Based on the solid-state NMR and MD analyses, the stabilization of olefins at the surface of silica is due to van der Waals interactions between the olefins and surface Si-OH and siloxane moieties; the increase in adsorption energy follows the olefin chain length and reflects the increasing contribution of dispersion forces. These observations elucidate qualitatively the difference in reactivity trends for $\mathbf{(\equiv SiO)_2Mo(=O)_2}$ compared to $\mathbf{Mo^+/SiO_2}$, the latter of which exhibits fewer isolated SiOH species that could act as olefin adsorption sites based on FTIR spectroscopy (Fig. S3).

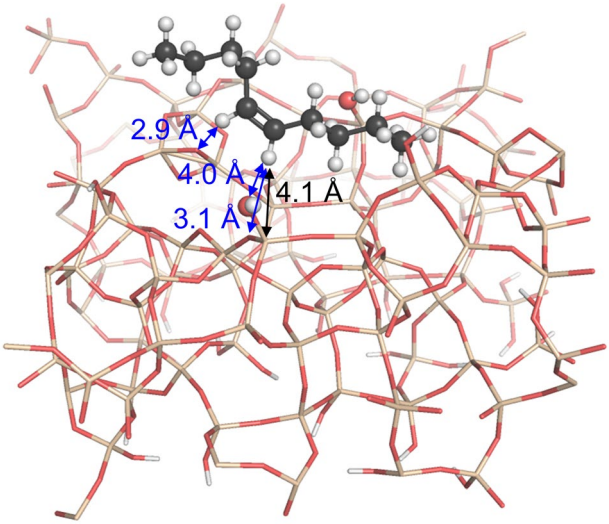

Figure 6. Representative conformation from MD simulations of an internal olefin (*cis*-5-decene) adsorbed on a model surface of dehydroxylated silica. The three shortest CH-O distances are indicated with blue arrows, and the black arrow indicates a CH-Si distance consistent with the 2D solid-state $^{29}Si\{^{1}H\}$ DNP-HETCOR NMR spectra in Figure 5a.

Conclusions

Silica-supported Mo-based catalysts show good activity and selectivity for low-temperature (< 100 °C) metathesis of linear α-olefins in the liquid phase, though this activity decreases sharply as a function of olefin chain length for supported Mo oxo species. In contrast, the molecularly defined alkylidene catalysts whether homogeneous or silica-supported display reaction rates less dependent on the olefin chain length. Solid-state NMR analyses of catalysts post-metathesis shows that the internal olefin products of metathesis adsorb on the catalyst support via interactions of olefinic moieties and surface Si-OH groups; this correlates with the decreased catalyst activity and also elucidates the higher performance of silica supported alkylidenes, which do not possess accessible OH groups. The observations are further corroborated by MD calculations. Overall, the analyses indicate that the metathesis rate of long-chain linear liquid a-olefins can be limited by

desorption of the bulky internal olefin products even in the condensed phase for both metathesis catalysts based on supported Mo oxides whether prepared via SOMC or classical wet impregnation approaches. This study also shows the utility of sensitivity-enhanced solid-state NMR as a tool for elucidating surface interactions in heterogeneous systems and understanding the molecular-scale origins of catalytic reaction properties. Finally, our studies demonstrate the advantages of SOMC and molecularly defined supported catalysts and offer insights into the origins of the lower activity for supported metathesis catalysts based on metal oxides, providing opportunities for the design of more active catalysts.

Author Contributions

Z.J.B, G.P., G.J.S., and C.C. conceptualized the study, designed the methodology, and analyzed the results. Z.J.B. and S.L.S. synthesized the heterogeneous catalysts and conducted the reactivity tests. M.J.B. and M.R.B. developed and synthesized the molecular alkylidene catalyst. M.B. conducted the MD simulations. Z.J.B. and C.C. co-wrote the manuscript. All authors discussed the results and commented on the manuscript during its preparation.

Conflicts of interest

There are no conflicts to declare.

Acknowledgements

This work was supported by BP plc. Z.J.B. gratefully acknowledges financial support from the Swiss National Science Foundation, Spark award CRSK-2_190322. M.B. would like to thank the ETH Zurich Grant program (ETH-44 18-1). M.R.B. acknowledges funding from the Deutsche

Forschungsgemeinschaft (DFG; German Research Foundation, project number 358283783 - CRC 1333).

Notes and references

1 R. H. Grubbs, *Angew. Chemie - Int. Ed.*, 2006, **45**, 3760–3765.

2 R. R. Schrock and A. H. Hoveyda, *Angew. Chemie - Int. Ed.*, 2003, **42**, 4592–4633.

3 M. R. Buchmeiser, S. Sen, J. Unold and W. Frey, *Angew. Chemie - Int. Ed.*, 2014, **53**, 9384–9388.

4 M. J. Koh, T. T. Nguyen, J. K. Lam, S. Torker, J. Hyvl, R. R. Schrock and A. H. Hoveyda, *Nature*, 2017, **542**, 80–85.

5 T. T. Nguyen, M. J. Koh, T. J. Mann, R. R. Schrock and A. H. Hoveyda, *Nature*, 2017, **552**, 347–354.

6 O. M. Ogba, N. C. Warner, D. J. O'Leary and R. H. Grubbs, *Chem. Soc. Rev.*, 2018, **47**, 4510–4544.

7 J. C. Mol, *J. Mol. Catal. A Chem.*, 2004, **213**, 39–45.

8 S. Lwin and I. E. Wachs, *ACS Catal.*, 2014, **4**, 2505–2520.

9 C. Copéret, A. Comas-Vives, M. P. Conley, D. P. Estes, A. Fedorov, V. Mougel, H. Nagae, F. Núnez-Zarur and P. A. Zhizhko, *Chem. Rev.*, 2016, **116**, 323–421.

10 C. Copéret, F. Allouche, K. W. Chan, M. P. Conley, M. F. Delley, A. Fedorov, I. B. Moroz, V. Mougel, M. Pucino, K. Searles, K. Yamamoto and P. A. Zhizhko, *Angew. Chemie - Int. Ed.*, 2018, **57**, 6398–6440.

11 P. A. Zhizhko, V. Mougel, J. De Jesus Silva and C. Copéret, Helv. Chim. Acta, 2018, **101**, e1700302.

12 M. Pucino, M. Inoue, C. P. Gordon, R. Schowner, L. Stöhr, S. Sen, C. Hegedüs, E. Robé, F. Tóth, M. R. Buchmeiser and C. Copéret, *Angew. Chemie - Int. Ed.*, 2018, **57**, 14566–14569.

13 P. A. Zhizhko, F. Toth, C. P. Gordon, K. W. Chan, W. C. Liao, V. Mougel and C. Copéret, *Helv. Chim. Acta*, 2019, **102**, e1900190.

14 J. De Jesus Silva, M. A. B. Ferreira, A. Fedorov, M. S. Sigman and C. Copéret, *Chem. Sci.*, 2020, **11**, 6717–6723.

15 V. Mougel, K. W. Chan, G. Siddiqi, K. Kawakita, H. Nagae, H. Tsurugi, K. Mashima, O. Safonova and C. Copéret, *ACS Cent. Sci.*, 2016, **2**, 569–576.

16 K. Yamamoto, K. W. Chan, V. Mougel, H. Nagae, H. Tsurugi, O. V. Safonova, K. Mashima and C. Copéret, *Chem. Commun.*, 2018, **54**, 3989–3992.

17 C. Copéret, Z. J. Berkson, K. W. Chan, J. de Jesus Silva, C. P. Gordon, M. Pucino and P. A. Zhizhko, *Chem. Sci.*, 2021, **12**, 3092–3115.

18 R. R. Schrock and C. Copéret, *Organometallics*, 2017, **36**, 1884–1892.

19 V. Mougel, C. B. Santiago, P. A. Zhizhko, E. N. Bess, J. Varga, G. Frater, M. S. Sigman and C. Copéret, *J. Am. Chem. Soc.*, 2015, **137**, 6699–6704.

20 M. Pucino, F. Zhai, C. P. Gordon, D. Mance, A. H. Hoveyda, R. R. Schrock and C. Copéret, *Angew. Chemie - Int. Ed.*, 2019, **58**, 11816–11819.

21 J. De Jesus Silva, M. Pucino, F. Zhai, D. Mance, Z. J. Berkson, D. F. Nater, A. H. Hoveyda, C. Copéret and R. R. Schrock, *Inorg. Chem.*, 2021, **60**, 6875–6880.

22 M. P. Conley, W. P. Forrest, V. Mougel, C. Copéret and R. R. Schrock, *Angew. Chemie - Int. Ed.*, 2014, **53**, 14221–14224.

23 M. Pucino, V. Mougel, R. Schowner, A. Fedorov, M. R. Buchmeiser, and C. Copéret, *Angew. Chemie - Int. Ed.*, 2016, **55**, 4300–4302.

24 N. Rendón, R. Berthoud, F. Blanc, D. Gajan, T. Maishal, J. M. Basset, C. Copéret, A. Lesage, L. Emsley, S. C. Marinescu, R. Singh and R. R. Schrock, *Chem. - A Eur. J.*, 2009, **15**, 5083–5089.

25 M. Pucino, W. C. Liao, K. W. Chan, E. Lam, R. Schowner, P. A. Zhizhko, M. R. Buchmeiser and C. Copéret, *Helv. Chim. Acta*, 2020, **6**, e2000072

26 O. L. Sydora, *Organometallics*, 2019, **38**, 997–1010.

27 W. Keim, *Angew. Chemie - Int. Ed.*, 2013, **52**, 12492–12496.

28 C. K. Rofer-DePoorter, *Chem. Rev.*, 1981, **81**, 447–474.

29 H. G. Stenger and C. N. Satterfleld, *Ind. Eng. Chem. Process Des. Dev.*, 1985, **24**, 411–415.

30 Y. Ishii, J. P. Yesinowski and R. Tycko, *J. Am. Chem. Soc.*, 2001, **123**, 2921–2922.

31 A. Venkatesh, M. P. Hanrahan and A. J. Rossini, *Solid State Nucl. Magn. Reson.*, 2017, **84**, 171–181.

32 A. J. Rossini, A. Zagdoun, M. Lelli, A. Lesage, C. Copéret and L. Emsley, *Acc. Chem. Res.*, 2013, **46**, 1942–1951.

33 M. Lelli, S. R. Chaudhari, D. Gajan, G. Casano, A. J. Rossini, O. Ouari, P. Tordo, A. Lesage and L. Emsley, *J. Am. Chem. Soc.*, 2015, **137**, 14558–14561.

34 W. C. Liao, B. Ghaffari, C. P. Gordon, J. Xu and C. Copéret, *Curr. Opin. Colloid Interface Sci.*, 2018, **33**, 63–71.

35 A. Finiels, F. Fajula and V. Hulea, *Catal. Sci. Technol.*, 2014, **4**, 2412–2426.

36 G. J. P. Britovsek, R. Malinowski, D. S. McGuinness, J. D. Nobbs, A. K. Tomov, A. W. Wadsley and C. T. Young, *ACS Catal.*, 2015, **5**, 6922–6925.

37 T. J. Donnelly, I. C. Yates and C. N. Satterfield, *Energy and Fuels*, 1988, **2**, 734–739.

38 A. Poater, X. Solans-Monfort, E. Clot, C. Copéret and O. Eisenstein, *J. Am. Chem. Soc.*, 2007, **129**, 8207–8216.

39 T. Saito, H. Nishiyama, H. Tanahashi, K. Kawakita, H. Tsurugi and K. Mashima, *J. Am. Chem. Soc.*, 2014, **136**, 5161–5170.

40 E. L. Lee and I. E. Wachs, *J. Phys. Chem. C*, 2007, **111**, 14410–14425.

41 S. Chempath, Z. Yihua and A. T. Bell, *J. Phys. Chem. C*, 2007, **111**, 1291–1298.

42 R. H. Crabtree, *The Organometallic Chemistry of the Transition Metals*, Hoboken, NJ, 6th Ed., 2014.

43 C. Copéret, *Beilstein J. Org. Chem.*, 2011, **7**, 13–21.

44 A. Salameh, A. Baudouin, J. M. Basset and C. Copéret, *Angew. Chemie - Int. Ed.*, 2008, **47**, 2117–2120.

45 M. R. Buchmeiser, S. Sen, C. Lienert, L. Widmann, R. Schowner, K. Herz, P. Hauser, W. Frey and D. Wang, *ChemCatChem*, 2016, **8**, 2710–2723.

46 S. Cadars, N. Mifsud, A. Lesage, J. D. Epping, N. Hedin, B. F. Chmelka and L. Emsley, *J. Phys. Chem. C*, 2008, **112**, 9145–9154.

47 T. Kobayashi, F. A. Perras, I. I. Slowing, A. D. Sadow and M. Pruski, *ACS Catal.*, 2015, **5**, 7055–7062.

48 T. Gutmann, P. B. Groszewicz and G. Buntkowsky, *Solid-state NMR of nanocrystals*, Elsevier Ltd., 1st edn., 2019, vol. 97.

49 L. Piveteau, T.-C. Ong, A. J. Rossini, L. Emsley, C. Copéret and M. V Kovalenko, *J. Am. Chem. Soc.*, 2015, **137**, 13964–13971.

50 L. Piveteau, T. C. Ong, B. J. Walder, D. N. Dirin, D. Moscheni, B. Schneider, J. Bär, L. Protesescu, N. Masciocchi, A. Guagliardi, L. Emsley, C. Copéret and M. V. Kovalenko, *ACS Cent. Sci.*, 2018, **4**, 1113–1125.

51 F. A. Perras, J. D. Padmos, R. L. Johnson, L.-L. L. Wang, T. J. Schwartz, T. Kobayashi, J. H. Horton, J. A. Dumesic, B. H. Shanks, D. D. Johnson and M. Pruski, *J. Am. Chem. Soc.*, 2017, **139**, 2702–2709.

52 A. G. M. M. Rankin, P. B. Webb, D. M. Dawson, J. Viger-gravel, B. J. Walder, L. Emsley and S. E. Ashbrook, *J. Phys. Chem. C*, 2017, **121**, 22977–22984.

53 R. P. Sangodkar, B. J. Smith, D. Gajan, A. J. Rossini, L. R. Roberts, G. P. Funkhouser, A. Lesage, L. Emsley and B. F. Chmelka, *J. Am. Chem. Soc.*, 2015, **137**, 8096–8112.

54 S. Smeets, Z. J. Berkson, D. Xie, S. I. Zones, W. Wan, X. Zou, M. F. Hsieh, B. F. Chmelka, L. B. McCusker and C. Baerlocher, *J. Am. Chem. Soc.*, 2017, **139**, 16803–16812.

55 Z. J. Berkson, M.-F. M. F. Hsieh, S. Smeets, D. Gajan, A. Lund, A. Lesage, D. Xie, S. I. Zones, L. B. McCusker, C. Baerlocher and B. F. B. F. Chmelka, *Angew. Chemie - Int. Ed.*, 2019, **58**, 6255–6259.

56 M. Valla, A. J. Rossini, M. Caillot, C. Chizallet, P. Raybaud, M. Digne, A. Chaumonnot, A. Lesage, L. Emsley, J. A. Van Bokhoven and C. Copéret, *J. Am. Chem. Soc.*, 2015, **137**, 10710–10719.

57 Z. Zhang, T. Xiao, H. Al-Megren, S. A. Aldrees, M. Al-Kinany, V. L. Kuznetsov, M. L. Kuznetsov and P. P. Edwards, *Chem. Commun.*, 2017, **53**, 4026–4029.

58 Y. Fang, S. Riahi, A. T. McDonald, M. Shrestha, D. J. Tobias and V. H. Grassian, *J. Phys. Chem. Lett.*, 2019, **10**, 468–473.

59 E. S. Frank, H. Fan, M. Shrestha, S. Riahi, D. J. Tobias and V. H. Grassian, *J. Phys. Chem. A*, 2020, **124**, 10592–10599.

60 F. Ziegler, H. Kraus, M. J. Benedikter, D. Wang, J. R. Bruckner, M. Nowakowski, K. Weißer, H. Solodenko, G. Schmitz, M. Bauer, N. Hansen and M. R. Buchmeiser, *ACS Catal.*, 2021, **11**, 11570–11578.

61 K. Amakawa, Y. Wang, J. Kröhnert, R. Schlögl and A. Trunschke, *Mol. Catal.*, 2019, **478**, 110580.

62 M.-J. Wang, S. Wolff and J.-B. Donnet, *Rubber Chem. Technol.*, 1991, **64**, 559–576.

63 A. Comas-Vives, *Phys. Chem. Chem. Phys.*, 2016, **18**, 7475–7482.